

Pressure-driven right-triangle shape superconductivity in bilayer nickelate $\text{La}_3\text{Ni}_2\text{O}_7$

Jingyuan Li¹, Peiyue Ma¹, Hengyuan Zhang¹, Xing Huang¹, Chaoxin Huang¹, Mengwu Huo¹, Deyuan Hu¹, Zixian Dong¹, Chengliang He¹, Jiahui Liao¹, Xiang Chen¹, Tao Xie¹, Hualei Sun^{2,*}, Meng Wang^{1,*}

¹Center for Neutron Science and Technology, Guangdong Provincial Key Laboratory of Magnetoelectric Physics and Devices, School of Physics, Sun Yat-Sen University, Guangzhou, Guangdong 510275, China

²School of Science, Sun Yat-Sen University, Shenzhen, Guangdong 518107, China

*Email: sunhlei@mail.sysu.edu.cn; wangmeng5@mail.sysu.edu.cn

Abstract: Here we report a comprehensive study of the crystal structure, resistivity, and alternating-current magnetic susceptibility in single crystals of $\text{La}_3\text{Ni}_2\text{O}_7$, with a hydrostatic pressure up to 104 GPa. X-ray diffraction measurements reveal a bilayer orthorhombic structure (space group $Amam$) at ambient pressure and a transformation into a tetragonal phase (space group $I4/mmm$) at a critical pressure of ~ 14 GPa. The transport measurements reveal a right-triangle shape superconducting region with a maximum T_c of 83 K at 18.0 GPa. The superconductivity is gradually suppressed when applying a higher pressure, but it can persist up to 90 GPa. Importantly, we measured the Meissner effect of superconductivity using an alternating-current magnetic susceptibility technique under pressure and estimated the maximum superconducting volume fraction of being 48% at 19.4 GPa. Thus, we demonstrate the bulk nature of superconductivity in the bilayer nickelate $\text{La}_3\text{Ni}_2\text{O}_7$ under high pressure. The intimate connection among the superconductivity, the oxygen content, and the tetragonal structure are discussed.

Seeking unconventional superconductivity in nickel-oxide materials has been a long-lasting topic due to the similar lattice and electronic structures with cuprates. Especially the Ni^+ in ReNiO_2 ($\text{Re} = \text{La}, \text{Nd}, \text{Sm}, \text{etc.}$) has the same spin configuration as Cu^{2+} in cuprates [1,2]. However, superconductivity wasn't realized in nickelates until the superconductivity with a transition temperature of $T_c = 15$ K was reported in $\text{Nd}_{0.8}\text{Sr}_{0.2}\text{NiO}_2$ thin film samples in 2019 [3-5]. Ni ions with a valence state close to Ni^+ and a spin $S=1/2$ in a planar coordination with oxygen ions were thought crucial for the emergence of superconductivity in nickelates [2,6]. The discovery of superconductivity in the Ruddlesden-Popper (RP) phase nickelate $\text{La}_3\text{Ni}_2\text{O}_7$ with $T_c \sim 80$ K has ignited renewed interest in the field of condensed matter physics [7-12]. The superconductivity was originally reported in the bilayer RP phase of $\text{La}_3\text{Ni}_2\text{O}_7$ with a '2222' stacking sequence of the NiO_6 octahedra between 14.0-43.5 GPa. The bilayer phase was

suggested to undergo a structural transition from a low-pressure orthorhombic *Amam* phase to a high-pressure orthorhombic *Fmmm* phase at room temperature, where the bonds of Ni-O-Ni along the *c* axis changed from 168° to 180° [7]. Scanning transmission electron microscopy (STEM) [13] and x-ray diffraction (XRD) measurements [14] confirmed the ‘2222’ stacking sequence on single crystals of La₃Ni₂O₇ grown by the high-pressure floating zone furnace and polycrystalline samples of La₃Ni₂O₇ [15] and La₂PrNi₂O₇ [16] grown by the sol-gel method. Oxygen vacancies were visualized on the inner apical oxygen site shared by two NiO₆ octahedra [13]. Further structural analysis under high pressure and low temperature revealed a tetragonal *I4/mmm* phase that corresponds to the compressed superconducting (SC) state [17]. Recently, a new structure of La₃Ni₂O₇ with an alternating monolayer-trilayer NiO₆ octahedra stacking sequence, denoted as the ‘1313’ phase, was identified [18-21]. It is unclear how the distinct structures might promote the high-*T_c* superconductivity in La₃Ni₂O₇.

The other enigmatic phenomena are the difficulty of realizing zero resistance and weakly suppressed *T_c* in La₃Ni₂O₇ under pressure [7,9-11]. Measurements using alternating-current (*ac*) magnetic susceptibility technique yield 1~20% SC volume fraction [7,11]. Such a low SC volume fraction and poor repeatability question the reliability of bulk superconductivity. A filamentary nature of the superconductivity was hence suggested in La₃Ni₂O₇ under pressure [11,15,19]. Recently, both zero resistance and the Meissner effect from direct-current (*dc*) magnetic susceptibility in the trilayer nickelate La₄Ni₃O₁₀ under pressure were reported, revealing a bulk superconductivity with *T_c* ~30 K [12,22-25]. Thus, it is of great importance to examine the bulk or filamentary nature of the superconductivity in the bilayer nickelate La₃Ni₂O₇.

In this work, we investigate the ambient and high-pressure structure of La₃Ni₂O₇, explore the electric properties, and clarify the controversy of bulk or filamentary superconductivity in compressed La₃Ni₂O₇. We show evidence that the high-pressure structural phase of La₃Ni₂O₇ belongs to the tetragonal *I4/mmm* space group at room temperature. Furthermore, the high-pressure transport measurements up to 104 GPa reveal a phase diagram of pressure-driven right-triangle shape superconductivity with a maximum *T_c* of 83 K. The SC phase is virtually suppressed above 90 GPa. The previously reported weakly insulating state at low pressures is not observed in the present study. The maximum SC volume fraction is estimated to be ~48% by measuring the high-pressure *ac* magnetic susceptibility, demonstrating bulk superconductivity in La₃Ni₂O₇. The validity of this method is confirmed by a parallel investigation of the polycrystalline Bi₂Sr₂CaCu₂O_{8+δ} (Bi-2212) samples.

The diamond anvil cell (DAC) electric transport and *ac* magnetic susceptibility measurements were performed on single crystals of La₃Ni₂O₇ from the same batch we investigated before [7,14,26]. It should be noted that a small amount of oxygen vacancies may be unavoidable due to the metastable structure and high oxygen pressure during the single crystal growth. Superconductivity was observed under high pressure

in all the samples we measured, suggesting a better sample quality which may be due to the fewer oxygen vacancies. Details of the analysis of the oxygen content have been discussed elsewhere and are beyond the scope of this work, we thus use $\text{La}_3\text{Ni}_2\text{O}_7$ to represent the composition of our sample for simplicity in this work [13]. For the XRD measurements, we measured the polycrystalline samples synthesized by the sol-gel method [15], and conducted the high-pressure synchrotron XRD measurements at the BL15U1 beamline at the Shanghai Synchrotron Radiation Facility (SSRF) with a wavelength of $\lambda = 0.6199 \text{ \AA}$. As a comparison, the Bi-2212 polycrystalline samples with $T_c = 77 \text{ K}$ were synthesized and measured using the *ac* magnetic susceptibility method to verify the accuracy of the SC volume fraction.

The structure of the $\text{La}_3\text{Ni}_2\text{O}_7$ samples at ambient pressure was first investigated. As shown in the simulated XRD patterns with $\text{Cu } K_\alpha$ radiation in Fig. 1a, the ‘2222’ phase and the ‘1313’ phase can be unambiguously distinguished. The experimental XRD pattern on our powder samples is consistent with the ‘2222’ bilayer structure. Figure 1b shows the single crystal XRD pattern of the (*H H L*) plane, where the (1 1 3) peak presents while the (1 1 2) peak is absent, consistent with the ‘2222’ bilayer structure. Previous STEM measurements on the same batch of single crystals also demonstrated the bilayer structure microscopically [13]. The high-pressure synchrotron XRD patterns at room temperature up to 29.8 GPa are shown in Fig. 1c. The separated reflections peaks near 13.21° can be indexed as (0 2 0) and (2 0 0) of the orthorhombic *Amam* space group, as shown in the inset of Fig. 1d (See supplementary Fig. S1 for lattice parameters). The two peaks merge at high pressure suggesting a structural transition to the *I4/mmm* space group [16]. Figure 1d shows the peak widths of (0 2 0)/(2 0 0) and (1 1 5) as a function of pressure. The peak widths of (1 1 5) represent the instrumental resolutions, which are broadened upon applying pressure. Below 14.1 GPa, the widths of (0 2 0)/(2 0 0) are broader than that of (1 1 5), indicating where the structural transition occurs. The *I4/mmm* space group also has flattened Ni-O-Ni bonds along the *c* axis, similar to the previously proposed *Fmmm* space group. Calculations of the electronic band structure based on the *I4/mmm* space group do not show a considerable distinction from that of the *Fmmm* space group [17].

The superconductivity was reported to abruptly emerge from either a weakly insulating state or a metallic state at ambient pressure [7-11]. A weakly pressure-dependent SC state and a strange metal normal state extend to 43.5 GPa. It is important to elucidate the evolution of the superconductivity under ultrahigh pressure. To justify the reliability of experimental results, we repeated high-pressure electric measurements on four different samples with a similar size of $30 \times 30 \times 10 \text{ }\mu\text{m}^3$ from the same batch (See supplementary Fig. S2a and S2b). KBr was adopted as a pressure-transmitting medium (PTM) in our measurements. Figure 2a shows the resistance at pressures from 0 to 104 GPa. At ambient pressure, the resistance shows a metallic behavior and an anomaly at $T^* \sim 140 \text{ K}$, which may be related to a density-wave transition [14,26-30]. By applying 0.9 GPa pressure in the DAC in run 1, the anomaly in resistance cannot be observed. The weakly insulating state at low pressures from the previous measurements

on single crystals with the size of $\sim 100 \times 100 \times 20 \text{ }\mu\text{m}^3$ is absent, suggesting that the weakly insulating state is likely an extrinsic property due to the sample or pressure inhomogeneity. A drop in resistance occurs at 8 K and 10.6 GPa, likely indicating the emergence of superconductivity. In contrast, the T_c is 50 K at 10.9 GPa in run 4 (See supplementary Fig. S1a). The dramatic difference in T_c can be ascribed to the fluctuation of superconductivity at the onset pressure. The T_c at 21.4 GPa is 73 K in run 1, while a residual resistance of 1 m Ω remains. The T_c s are suppressed gradually until they cannot be identified at 91.5 GPa and above. The strange metal behavior persists up to 104 GPa which is the highest pressure achieved in the current measurements.

Figure 2b shows the resistance for run 2. The onset T_c is 83 K at 18 GPa which is higher than previous reports (See supplementary Fig. S2c) [7]. Figure 2c shows the high-pressure transport data of run 3. A SC transition with an onset $T_c \sim 70$ K appears at 12.4 GPa and is enhanced to 75 K at 18.0 GPa. A remarkable zero resistance appears below 12 K at both 18.0 and 21.6 GPa (Fig. 2d). The zero-resistance state is realized with the solid PTM, indicating a good sample quality. The SC transition is gradually suppressed by the external field up to 14 T, as shown in Fig. 2e (See supplementary Fig. S2b). The various T_c s indicate that the oxygen content influences the superconductivity in compressed $\text{La}_3\text{Ni}_2\text{O}_7$ and the higher T_c s are accessible by optimizing the composition.

The electric transport results measured under high pressure are summarized in Fig. 3. The T_c^{onset} is defined as the onset SC transition temperature, while the T_c^{mid} is defined as the temperature where the resistance is in the middle of that at the onset T_c and 2 K. The background color scale is the relative change of the resistance to that at 150 K in run 1. Superconductivity emerges near 10 GPa and is enhanced by the *Amam* to *I4/mmm* structural transition. The reasons may be due to a Fermi surface reconstruction or enhancement of the interlayer magnetic exchange coupling coincident with the first order structural transition [31-39,61-63]. The T_c abruptly reaches a maximum of 83 K at 18 GPa and then decreases with increasing pressure, highlighting the right-triangle-like feature of the superconductivity in $\text{La}_3\text{Ni}_2\text{O}_7$ under pressure. The T_c^{onset} drops to 38 K at 80.2 GPa. These features indicate a robust bulk SC phase in $\text{La}_3\text{Ni}_2\text{O}_7$.

To further investigate the nature of the superconductivity of $\text{La}_3\text{Ni}_2\text{O}_7$ under pressure, a high-pressure *ac* magnetic susceptibility measurement system (HPMS) is employed to measure the Meissner effect of superconductivity [40-43]. The HPMS adopts a symmetric DAC with anvils of 500 μm culets, as shown in Fig. 4a. The sample was loaded into the hole of a non-magnetic BeCu gasket. The coil system was placed on the gasket, with a 100-turn pick-up coil wound around the sample. To reduce the temperature-dependent background of the DAC, an identical compensation coil was oppositely connected to the pick-up coil. An alternating field was generated by a 100-turn excitation coil outside the pick-up and compensation coils. The inner diameters of the excitation coil and pick-up coil are 5.8 and 2.0 mm, respectively. The length of the coil is approximately 1.0 mm. When the sample is cooled below T_c , the Meissner effect

forces magnetic flux out of the pick-up coil. A drop in the real part of the induced voltage is expected [40-42]. The magnitude of the drop measured by such a coil can be calculated by the formula $\Delta\chi' = \frac{\pi f \alpha H V N}{R(1-D)} \chi$ [41,44], where f , H , and V are the frequency of the alternating field, the magnitude of the generated field, and the sample volume, respectively. Note the sample is in the center of the pick-up coil, which is off the center of the excitation coil. N and R are the number of turns and radius of the pick-up coil. α is a sample-dependent coefficient defined as $\alpha = 1/\sqrt{1 + (L/R)^2}$, where $2L$ is the length of the coil. D is the geometry demagnetization factor assumed as $D = 1 - [2h/(\pi d)][\ln(8d/h) - 1]$ [45] for a cylindrical sample, in which h and d are the height and diameter of the sample, respectively. χ is -1 for a superconductor with 100% SC volume fraction. To enhance the detected signal, a pre-amplifier with a 500 magnification was connected to the circuit outside of the cryostat.

To check the validity of the HPMS, we measured a polycrystalline Bi-2212 sample as a reference. The dc magnetic susceptibility of Bi-2212 was measured, yielding a SC transition at $T_c = 77$ K and a volume fraction of 59% after considering the demagnetization factor [Fig. 4b]. The Bi-2212 sample with a size of $h = 20$ μm and $d = 180$ μm was loaded in the pick-up coil of HPMS. A current of 50 mA was applied in the excitation coil, inducing a magnetic field of ~ 20 Oe at the sample position [46]. To avoid changing the SC properties of Bi-2212 [47], we measured the superconductivity using the HPMS near ambient pressure with selected frequencies of the alternating currents. Sharp transitions around 77 K can be observed after subtraction of a linear background, as shown in Fig. 4c (See supplementary Fig. S4). A slight shift of T_c as changing frequency may be attributed to the pressure relaxation upon repeating the cooling and warming procedures because the T_c s vary ~ 2 K for repeated measurements with 393 Hz alternating excitation currents. The SC volume fractions calculated from the measured $\Delta\chi'_{2212}$ result in 40% (averaged for three times measurements), 43%, 50%, and 42% for the alternating current frequencies of 393, 423, 460, and 560 Hz respectively. The induced change of the voltage of the pick-up coil seems to saturate at $f = 560$ Hz. The result for $f = 460$ Hz is the closest to the dc magnetic susceptibility measurements, confirming the validity of the calculations from the HPMS.

We then loaded a similar size of $\text{La}_3\text{Ni}_2\text{O}_7$ single crystals to the same HPMS and conducted the measurements at 5.5, 19.4, and 23.4 GPa. Figure 4d shows the ac susceptibility measured at 5.5 GPa. Interestingly, weak drops of $\Delta\chi'$ can be identified at around 81 K for 393 and 423 Hz, in contrast to the absence of an anomaly at 373 Hz. The appearance of the SC-like transition at 5.5 GPa may be related to the contraction of the anvil cell used in the HPMS, where the real pressure is close to the onset pressure of superconductivity [15,19]. At 19.4 GPa as shown in Fig. 4e, $\text{La}_3\text{Ni}_2\text{O}_7$ has shown good superconductivity after the structural transition, the SC transitions can be observed at 76-80 K for all the frequencies. The calculated SC volume fractions are 21%, 22%, 48%, and 42% for the current frequencies of 393, 423, 460, and 560 Hz.

The measurements at 23.4 GPa are shown in Fig. 4f. The T_c s are suppressed weakly. However, the SC transition is almost absent for the frequency of 393 Hz. The corresponding SC volume fractions at 423, 460, and 560 Hz are 13%, 28%, and 23%, respectively. Our data reveal the resultant SC volume fraction of $\text{La}_3\text{Ni}_2\text{O}_7$ varies with pressure and the excitation coil frequency.

The emergence of superconductivity in $\text{La}_3\text{Ni}_2\text{O}_7$ under high pressure exhibits sample and pressure homogeneity dependence [7-9,11]. Both zero resistance and *ac* diamagnetic susceptibility have been achieved in single crystals of $\text{La}_3\text{Ni}_2\text{O}_7$. However, the zero resistance can only be observed for small samples with typical sizes of $30 \times 30 \times 10 \mu\text{m}^3$ or smaller. The SC volume fraction estimated from the *ac* magnetic susceptibility measurements varies from previously obtained several percent to the maximum of 48% in this work, which is likely a result of the oxygen vacancy and pressure inhomogeneity. This conjecture is supported by the STEM measurements, which directly reveal various distributions of the oxygen vacancies, especially at the inner apical oxygen site [13]. The inner apical oxygen is directly involved in the superexchange magnetic interactions of the two nickel ions along the *c*-axis and affects the splitting of the bonding and antibonding states of the $3d_{z^2}$ orbitals [7,37,48-51]. The interlayer coupling plays an important role in the superconductivity in compressed $\text{La}_3\text{Ni}_2\text{O}_7$ according to extensive theoretical analysis [31,32,34,52-55,61-63]. Inelastic neutron scattering [56] and resonance inelastic x-ray scattering measurements [29] indeed reveal a strong interlayer coupling in $\text{La}_3\text{Ni}_2\text{O}_7$ compared to the dominant intralayer couplings in copper-based [57] and iron-based superconductors [58]. It is reasonable to assume that the inner apical oxygen vacancies will suppress the superconductivity in the bilayer nickelate under pressure.

Compared to La_2NiO_4 and $\text{La}_4\text{Ni}_3\text{O}_{10}$, the bilayer $\text{La}_3\text{Ni}_2\text{O}_7$ is a metastable phase with a narrower oxygen pressure window of 10-18 bar during the single crystal growth [59]. This complicates the sample synthesis, and a sample inhomogeneity is hard to avoid. Further, the quality of the single crystals using the optical floating zone method also depends on the speed of movements and rotations of the feed and seed rods, the diameter of the rods, and the stability of the melting zone. The other intergrowth phases such as La_2NiO_4 , $\text{La}_4\text{Ni}_3\text{O}_{10}$, and some other stacking sequences are also possible [18,21,60]. Even for successful growth, the inhomogeneity and vacancies of oxygen are inevitable because of the valence state of $\text{Ni}^{2.5+}$ in $\text{La}_3\text{Ni}_2\text{O}_7$. For samples with more oxygen vacancies, the SC volume fraction can be low, and the superconductivity behaves like filamentary. However, the reported STEM data [26] and the *ac* magnetic susceptibility in this work demonstrate that samples with a large SC volume fraction and zero resistance are achievable. The intimate relationship between pressure homogeneity and superconductivity in $\text{La}_3\text{Ni}_2\text{O}_7$ may be ascribed to the crucial role of the tetragonal $I4/mmm$ space group in the SC state and the bilayer structure. The abrupt emergence of superconductivity (the right-triangle shape) is intimately related to the first order structural transition.

In conclusion, we have demonstrated the $\text{La}_3\text{Ni}_2\text{O}_7$ samples we grew belong to the ‘2222’ bilayer phase. The structure that corresponds to the superconductivity under high pressures is in the tetragonal $I4/mmm$ space group. A pressure-temperature phase diagram from ambient pressure to 104 GPa is obtained, displaying a right-triangle shape SC region that ends up at 90 GPa, different from that of carrier-doped or pressure-induced dome-shaped SC phase diagram in both cuprates and iron pnictides. The Meissner effect is measured, and the calculated maximum SC volume fraction is 48% at 19.4 GPa, suggesting the bulk nature of superconductivity. These findings provide important insights into the current confusion about the superconductivity in compressed $\text{La}_3\text{Ni}_2\text{O}_7$.

Work at Sun Yat-Sen University was supported by the National Key Research and Development Program of China (grant nos. 2023YFA1406500 and 2023YFA1406002), the National Natural Science Foundation of China (grant nos. 12174454 and 12304187), the Guangdong Basic and Applied Basic Research Foundation (grant No. 2021B1515120015), the Guangzhou Basic and Applied Basic Research Funds (grant nos. 2024A04J6417 and 2024A04J4024), the open research fund of Songshan Lake Materials Laboratory (grant no. 2023SLABFN30), the Fundamental Research Funds for the Central Universities, Sun Yat-sen University (grant no. 23qnp57), and the Guangdong Provincial Key Laboratory of Magnetoelectric Physics and Devices (grant no. 2022B1212010008). We also thank the BL15U1 station in Shanghai Synchrotron Radiation Facility (SSRF) for the help in high-pressure structural characterizations and the School of Physics and Optoelectronics, South China University of Technology for supporting the high-pressure *ac* magnetic susceptibility measurements.

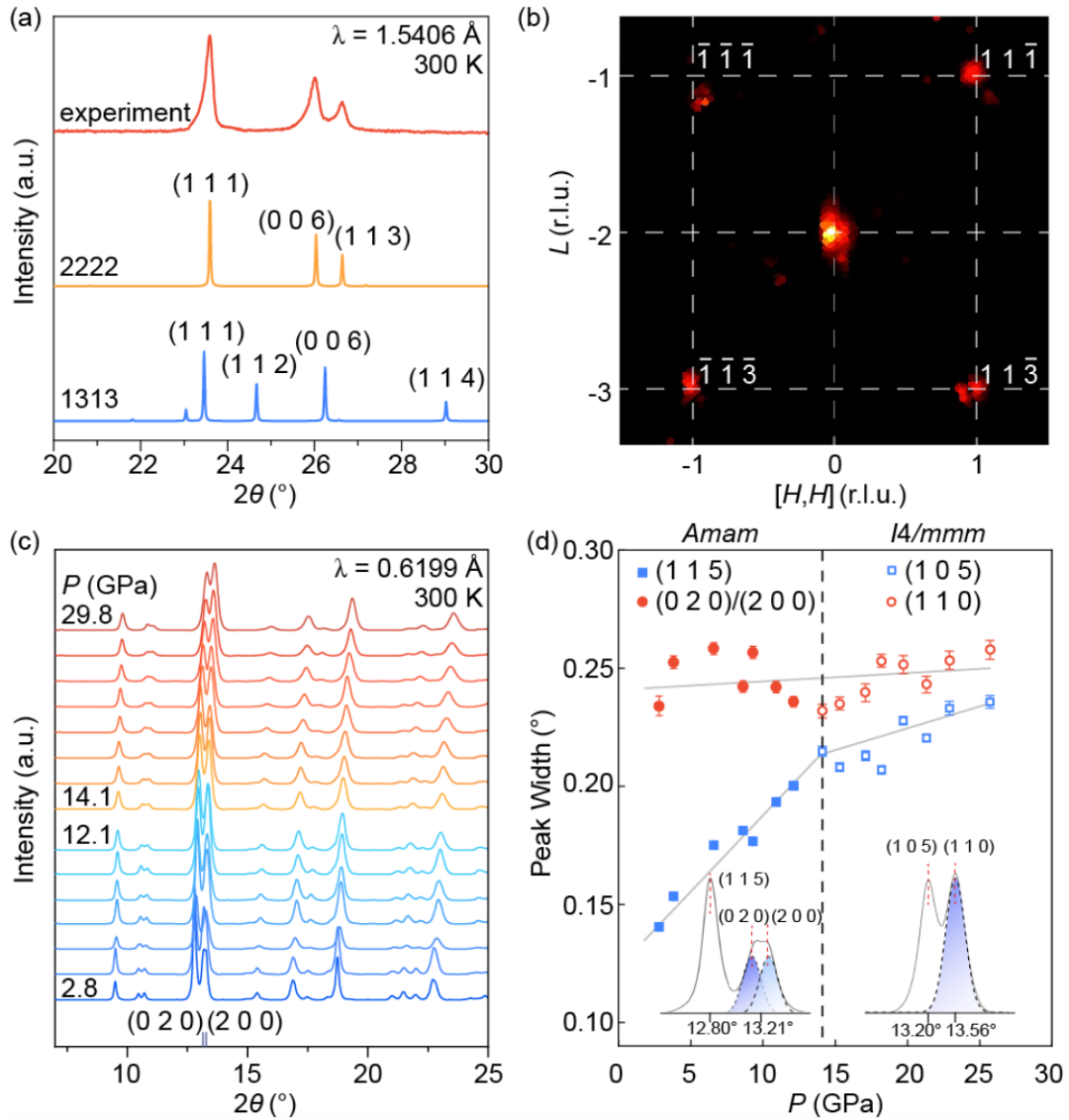


FIG. 1. Structural characterizations of $\text{La}_3\text{Ni}_2\text{O}_7$. (a) Powder X-ray diffraction (XRD) pattern at ambient pressure (red line). The simulated XRD patterns of the 2222-phase (orange line) and 1313-phase (blue line) are shown below for comparison. (b) A slice of single crystal XRD pattern in the $(H H L)$ plane. (c) Synchrotron XRD patterns under different pressures from 2.8 to 29.8 GPa. (d) Pressure dependence of the peak widths of (0 2 0), (2 0 0), and (1 1 5) in the $Amam$ space group. A merging of the peak widths at 14.1 GPa signals a structural transition from the $Amam$ phase to the tetragonal $I4/mmm$ phase. The reflection indexes of (1 1 5) and (0 2 0)/(2 0 0) change to (1 0 5) and (1 1 0) in the $I4/mmm$ space group. The insets are the zoomed-in experimental data. The solid lines are a guide to the eyes.

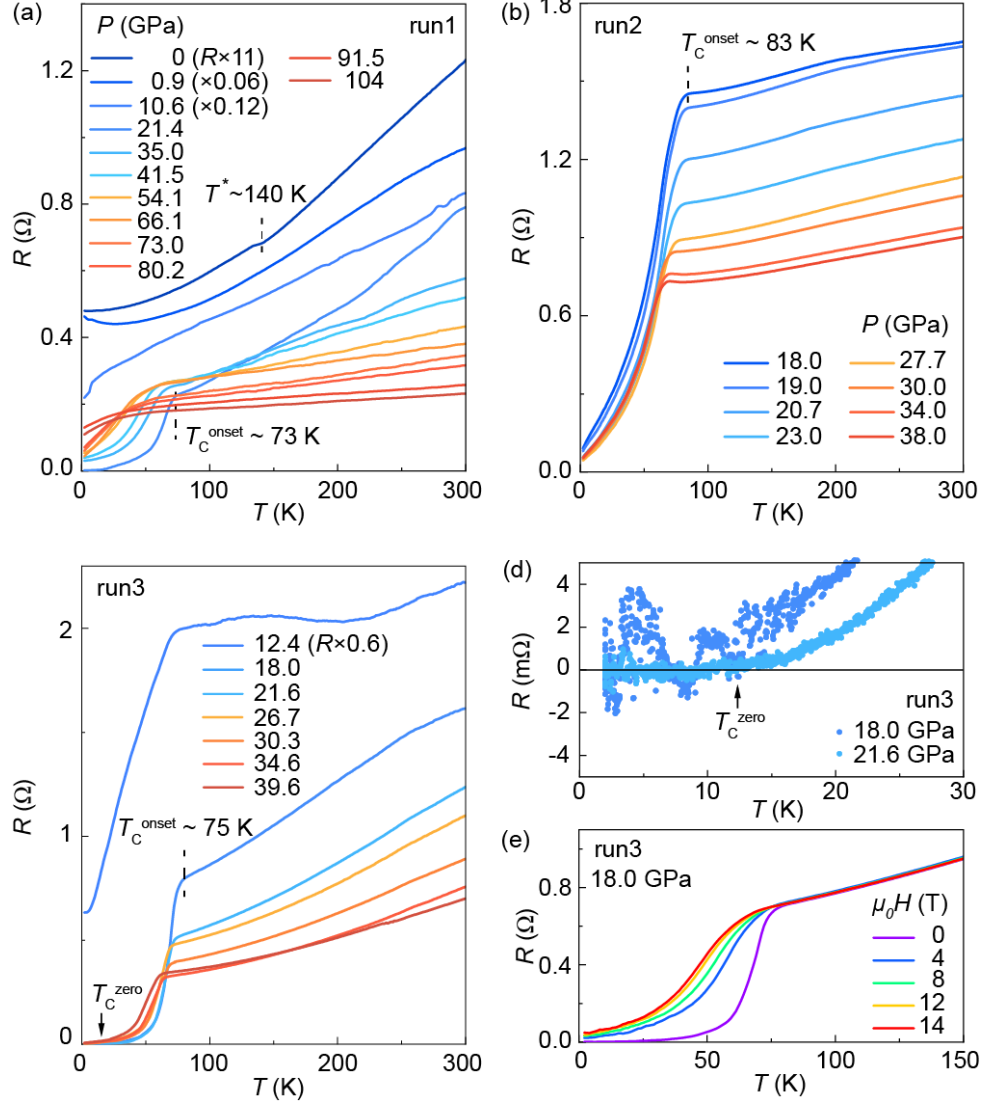


FIG. 2. Temperature dependence of the in-plane resistance of $\text{La}_3\text{Ni}_2\text{O}_7$ under various pressures. (a)-(b) High-pressure resistance curves of run 1 and run 2 measurements. The resistance of $\text{La}_3\text{Ni}_2\text{O}_7$ from ambient pressure to 104 GPa is measured in run 1. A $T_c^{\text{onset}} \sim 83$ K is observed in run 2, breaking the record of the highest $T_c^{\text{onset}} \sim 80$ K in previous measurements on single crystals. (c) High-pressure resistance of run 3 measurements. (d) A zoom-in view of the resistance curves of run 3 below 30 K. The achievement of zero resistance is clearly shown. (e) Field-dependent resistance curves at 18.0 GPa of run3 measurements.

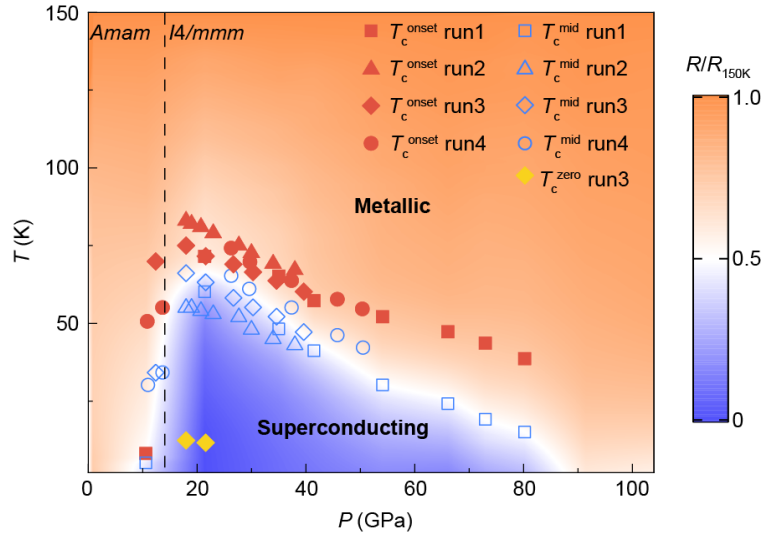


FIG. 3. The superconducting phase diagram of $\text{La}_3\text{Ni}_2\text{O}_7$ single crystals under pressures ranging from ambient pressure to 104 GPa. The red solid symbols represent the onset temperatures of superconductivity T_c^{onset} obtained from four runs. The blue hollow symbols represent the middle temperatures T_c^{mid} of the SC transition defined by the temperature corresponding to the resistance of $R_{\text{mid}} = (R_{\text{onset}} + R_{2K})/2$. The yellow rhombuses mark the zero resistance temperatures T_c^{zero} of run 3. Data points obtained from different testing rounds are denoted as different shapes. A dome-shaped evolution of T_c is obtained within the pressure range. The color of the ground shows the data of run 1.

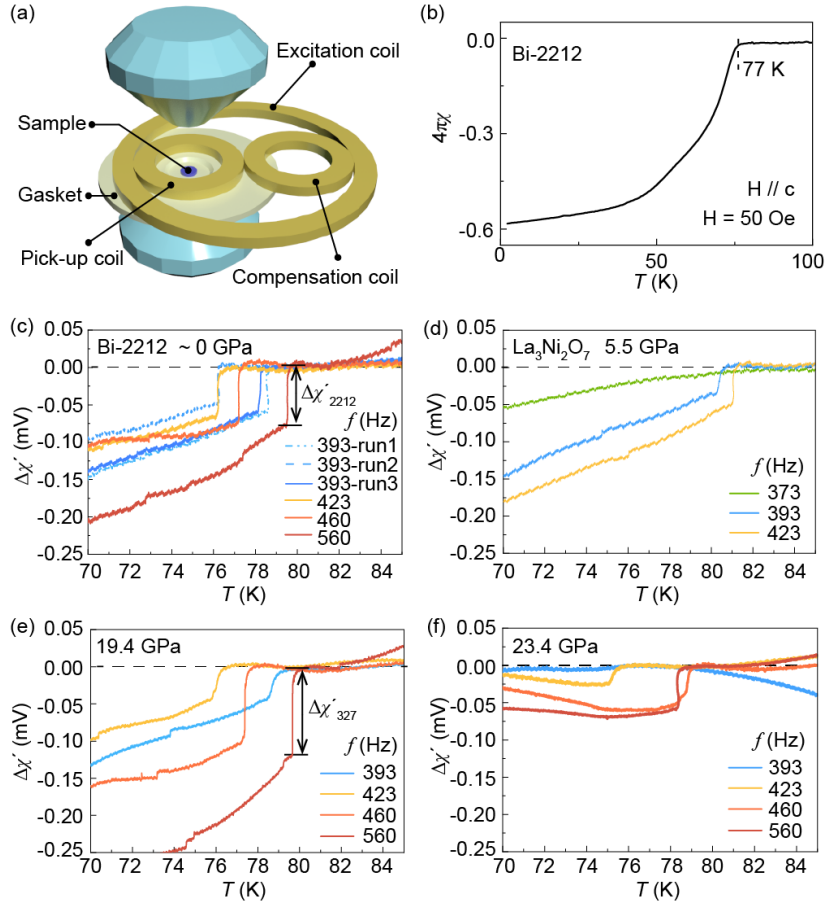


FIG. 4. (a) Schematic of the experimental set-up of the high-pressure *ac* magnetic susceptibility measurement system. (b) The *dc* magnetic susceptibility of Bi-2212, yielding $T_c = 77$ K and a superconducting volume fraction of 59%. (c) Frequency dependence of the real parts of the *ac* susceptibility of Bi-2212 at ambient pressure. The diamagnetic drop $\Delta\chi'_{2212}$ tends to increase with the increasing frequency. (d)-(f) Frequency dependence of the real parts of the *ac* susceptibility of $\text{La}_3\text{Ni}_2\text{O}_7$ at 5.5, 19.4, and 23.4 GPa, respectively. Different frequencies from 373 to 560 Hz are measured. The rapid drops can be attributed to the Meissner effect of superconductivity.

References

- [1] I. Bozovic, G. Logvenov and V. Butko, Atomic-layer engineering of nickelates (in search of novel superconductors), *Physica C* **615**, 6, 1354388 (2023).
- [2] V. I. Anisimov, D. Bukhvalov and T. M. Rice, Electronic structure of possible nickelate analogs to the cuprates, *Physical Review B* **59**, 7901 (1999).
- [3] D. F. Li, K. Lee, B. Y. Wang, M. Osada, S. Crossley, H. R. Lee, Y. Cui, Y. Hikita and H. Y. Hwang, Superconductivity in an infinite-layer nickelate, *Nature* **572**, 624 (2019).
- [4] S. Zeng, C. S. Tang, X. Yin, C. Li, M. Li, Z. Huang, J. Hu, W. Liu, G. J. Omar, H. Jani *et al.*, Phase diagram and superconducting dome of infinite-Layer Nd_{1-x}Sr_xNiO₂ thin films, *Physical Review Letters* **125**, 7, 147003 (2020).
- [5] M. Osada, B. Y. Wang, B. H. Goodge, K. Lee, H. Yoon, K. Sakuma, D. Li, M. Miura, L. F. Kourkoutis and H. Y. Hwang, A Superconducting Praseodymium Nickelate with Infinite Layer Structure, *Nano Letters* **20**, 5735 (2020).
- [6] A. S. Botana and M. R. Norman, Similarities and differences between LaNiO₂ and CaCuO₂ and implications for superconductivity, *Physical Review X* **10**, 011024 (2020).
- [7] H. L. Sun, M. W. Huo, X. W. Hu, J. Y. Li, Z. J. Liu, Y. F. Han, L. Y. Tang, Z. Q. Mao, P. T. Yang, B. S. Wang *et al.*, Signatures of superconductivity near 80 K in a nickelate under high pressure, *Nature* **621**, 493 (2023).
- [8] Y. Zhang, D. Su, Y. Huang, H. Sun, M. Huo, Z. Shan, K. Ye, Z. Yang, R. Li, M. Smidman *et al.*, High-temperature superconductivity with zero-resistance and strange metal behavior in La₃Ni₂O₇, arXiv:2307.14819 (2023).
- [9] J. Hou, P. T. Yang, Z. Y. Liu, J. Y. Li, P. F. Shan, L. Ma, G. Wang, N. N. Wang, H. Z. Guo, J. P. Sun *et al.*, Emergence of High-Temperature Superconducting Phase in Pressurized La₃Ni₂O₇ Crystals, *Chinese Physics Letters* **40**, 6, 117302 (2023).
- [10] M. X. Zhang, C. Y. Pei, Q. Wang, Y. Zhao, C. H. Li, W. Z. Cao, S. H. Zhu, J. F. Wu and Y. P. Qi, Effects of pressure and doping on Ruddlesden-Popper phases La_{n+1}Ni_nO_{3n+1}, *J. Mater. Sci. Technol.* **185**, 147 (2024).
- [11] Y. Zhou, J. Guo, S. Cai, H. Sun, P. Wang, J. Zhao, J. Han, X. Chen, Q. Wu and Y. Ding, Evidence of filamentary superconductivity in pressurized La₃Ni₂O₇ single crystals, arXiv:2311.12361 (2023).
- [12] H. Sakakibara, M. Ochi, H. Nagata, Y. Ueki, H. Sakurai, R. Matsumoto, K. Terashima, K. Hirose, H. Ohta, M. Kato *et al.*, Theoretical analysis on the possibility of superconductivity in the trilayer Ruddlesden-Popper nickelate La₄Ni₃O₁₀ under pressure and its experimental examination: comparison with La₃Ni₂O₇, *Physical Review B* **109**, 144511 (2024).
- [13] Z. Dong, M. Huo, J. Li, J. Li, P. Li, H. Sun, Y. Lu, M. Wang, Y. Wang and Z. Chen, Visualization of oxygen vacancies and self-doped ligand holes in La₃Ni₂O_{7-δ}, arXiv:2312.15727 (2023).
- [14] Z. J. Liu, H. L. Sun, M. W. Huo, X. Y. Ma, Y. Ji, E. K. Yi, L. S. Li, H. Liu, J. Yu, Z. Y. Zhang *et al.*, Evidence for charge and spin density waves in single crystals of La₃Ni₂O₇ and La₃Ni₂O₆, *Sci. China-Phys. Mech. Astron.* **66**, 7, 217411 (2023).
- [15] G. Wang, N. N. Wang, X. L. Shen, J. Hou, L. Ma, L. F. Shi, Z. A. Ren, Y. D. Gu, H. M. Ma, P. T. Yang *et al.*, Pressure-induced superconductivity in polycrystalline La₃Ni₂O_{7-δ},

Physical Review X **14**, 8, 011040 (2024).

[16] G. Wang, N. Wang, Y. Wang, L. Shi, X. Shen, J. Hou, H. Ma, P. Yang, Z. Liu and H. Zhang, Observation of high-temperature superconductivity in the high-pressure tetragonal phase of $\text{La}_2\text{PrNi}_2\text{O}_7-\delta$, arXiv:2311.08212 (2023).

[17] L. H. Wang, Y. Li, S. Y. Xie, F. Y. Liu, H. L. Sun, C. X. Huang, Y. Gao, T. Nakagawa, B. Y. Fu, B. Dong *et al.*, Structure responsible for the superconducting state in $\text{La}_3\text{Ni}_2\text{O}_7$ at high-pressure and low-temperature conditions, J. Am. Chem. Soc. **146**, 7506 (2024).

[18] X. Chen, J. Zhang, A. S. Thind, S. Sharma, H. LaBollita, G. Peterson, H. Zheng, D. P. Phelan, A. S. Botana and R. F. Klie, Polymorphism in the Ruddlesden–Popper nickelate $\text{La}_3\text{Ni}_2\text{O}_7$: discovery of a hidden phase with distinctive layer stacking, J. Am. Chem. Soc. **146**, 3640 (2024).

[19] P. Puphal, P. Reiss, N. Enderlein, Y.-M. Wu, G. Khaliullin, V. Sundaramurthy, T. Priessnitz, M. Knauft, L. Richter and M. Isobe, Unconventional crystal structure of the high-pressure superconductor $\text{La}_3\text{Ni}_2\text{O}_7$, arXiv:2312.07341 (2023).

[20] S. N. Abadi, K. J. Xu, E. G. Lomeli, P. Puphal, M. Isobe, Y. Zhong, A. V. Fedorov, S. K. Mo, M. Hashimoto, D. H. Lu *et al.*, Electronic structure of the alternating monolayer-trilayer phase of $\text{La}_3\text{Ni}_2\text{O}_7$, arXiv:2402.07143.

[21] H. Z. Wang, L. Chen, A. Rutherford, H. D. Zhou and W. W. Xie, Long-range structural order in a hidden phase of Ruddlesden–Popper bilayer nickelate $\text{La}_3\text{Ni}_2\text{O}_7$, Inorg. Chem. **63**, 5020 (2024).

[22] Y. Zhu, E. Zhang, B. Pan, X. Chen, L. Chen, H. Ren, F. Liu, J. Wang, D. Jia, H. Wo *et al.*, Signatures of superconductivity in trilayer $\text{La}_4\text{Ni}_3\text{O}_{10}$ single crystals, arXiv:2311.07353 (2023).

[23] Q. Li, Y. J. Zhang, Z. N. Xiang, Y. H. Zhang, X. Y. Zhu and H. H. Wen, Signature of superconductivity in pressurized $\text{La}_4\text{Ni}_3\text{O}_{10}$, Chinese Physics Letters **41**, 8, 017401 (2024).

[24] M. Zhang, C. Pei, X. Du, Y. Cao, Q. Wang, J. Wu, Y. Li, Y. Zhao, C. Li, W. Cao *et al.*, Superconductivity in trilayer nickelate $\text{La}_4\text{Ni}_3\text{O}_{10}$ under pressure, arXiv:2311.07423 (2023).

[25] J. Y. Li, C. Q. Chen, C. X. Huang, Y. F. Han, M. W. Huo, X. Huang, P. Y. Ma, Z. Y. Qiu, J. F. Chen, X. W. Hu *et al.*, Structural transition, electric transport, and electronic structures in the compressed trilayer nickelate $\text{La}_4\text{Ni}_3\text{O}_{10}$, Sci. China-Phys. Mech. Astron. **67**, 7, 117403 (2024).

[26] Z. Dan, Y. Zhou, M. Huo, Y. Wang, L. Nie, M. Wang, T. Wu and X. Chen, Spin-density-wave transition in double-layer nickelate $\text{La}_3\text{Ni}_2\text{O}_7$, arXiv:2402.03952 (2024).

[27] G. Q. Wu, J. J. Neumeier and M. F. Hundley, Magnetic susceptibility, heat capacity, and pressure dependence of the electrical resistivity of $\text{La}_3\text{Ni}_2\text{O}_7$ and $\text{La}_4\text{Ni}_3\text{O}_{10}$, Physical Review B **63**, 5, 245120 (2001).

[28] Z. Liu, M. Huo, J. Li, Q. Li, Y. Liu, Y. Dai, X. Zhou, J. Hao, Y. Lu, M. Wang *et al.*, Electronic correlations and energy gap in the bilayer nickelate $\text{La}_3\text{Ni}_2\text{O}_7$, arXiv:2307.02950 (2023).

[29] X. Chen, J. Choi, Z. Jiang, J. Mei, K. Jiang, J. Li, S. Agrestini, M. Garcia-Fernandez, X. Huang, H. Sun *et al.*, Electronic and magnetic excitations in $\text{La}_3\text{Ni}_2\text{O}_7$, arXiv:2401.12657 (2024).

[30] K. Chen, X. Liu, J. Jiao, M. Zou, Y. Luo, Q. Wu, N. Zhang, Y. Guo and L. Shu, Evidence of spin density waves in $\text{La}_3\text{Ni}_2\text{O}_7-\delta$, arXiv:2311.15717 (2023).

- [31] Y.-f. Yang, G.-M. Zhang and F.-C. Zhang, Interlayer valence bonds and two-component theory for high-T_c superconductivity of La₃Ni₂O₇ under pressure, *Physical Review B* **108**, L201108 (2023).
- [32] C. Lu, Z. Pan, F. Yang and C. Wu, Interlayer-Coupling-Driven High-Temperature Superconductivity in La₃Ni₂O₇ under Pressure, *Physical Review Letters* **132**, 146002 (2024).
- [33] H. Sakakibara, N. Kitamine, M. Ochi and K. Kuroki, Possible high T_c superconductivity in La₃Ni₂O₇ under high pressure through manifestation of a nearly half-filled bilayer Hubbard model, *Physical Review Letters* **132**, 106002 (2024).
- [34] Z. Luo, X. Hu, M. Wang, W. Wu and D.-X. Yao, Bilayer two-orbital model of La₃Ni₂O₇ under pressure, *Physical Review Letters* **131**, 126001 (2023).
- [35] V. Christiansson, F. Petocchi and P. Werner, Correlated electronic structure of La₃Ni₂O₇ under pressure, *Physical Review Letters* **131**, 6, 206501 (2023).
- [36] Y. Zhang, L. F. Lin, A. Moreo, T. A. Maier and E. Dagotto, Structural phase transition, s_±-wave pairing, and magnetic stripe order in bilayered superconductor La₃Ni₂O₇ under pressure, *Nature Communications* **15**, 11, 2470 (2024).
- [37] K. Jiang, Y. Wang, Z. Wang, F.-C. Zhang and J. Hu, Electronic structure and superconductivity in bilayer La₃Ni₂O₇, arXiv:2401.15097 (2024).
- [38] W. Wú, Z. H. Luo, D. X. Yao and M. Wang, Superexchange and charge transfer in the nickelate superconductor La₃Ni₂O₇ under pressure, *Sci. China-Phys. Mech. Astron.* **67**, 8, 117402 (2024).
- [39] Z. Fan, J.-F. Zhang, B. Zhan, D. Lv, X.-Y. Jiang, B. Normand and T. Xiang, Superconductivity in nickelate and cuprate superconductors with strong bilayer coupling, arXiv:2312.17064 (2023).
- [40] Y. A. Timofeev, V. V. Struzhkin, R. J. Hemley, H. K. Mao and E. A. Gregoryanz, Improved techniques for measurement of superconductivity in diamond anvil cells by magnetic susceptibility, *Rev. Sci. Instrum.* **73**, 371 (2002).
- [41] M. Debessai, J. J. Hamlin and J. S. Schilling, Comparison of the pressure dependences of T_c in the trivalent d-electron superconductors Sc, Y, La, and Lu up to megabar pressures, *Physical Review B* **78**, 10, 064519 (2008).
- [42] X. L. Huang, X. Wang, D. F. Duan, B. Sundqvist, X. Li, Y. P. Huang, H. Y. Yu, F. F. Li, Q. Zhou, B. B. Liu *et al.*, High-temperature superconductivity in sulfur hydride evidenced by alternating-current magnetic susceptibility, *Natl. Sci. Rev.* **6**, 713 (2019).
- [43] L. L. Sun, X. J. Chen, J. Guo, P. W. Gao, Q. Z. Huang, H. D. Wang, M. H. Fang, X. L. Chen, G. F. Chen, Q. Wu *et al.*, Re-emerging superconductivity at 48 kelvin in iron chalcogenides, *Nature* **483**, 67 (2012).
- [44] J. J. H. Hamlin, Thesis, 2007.
- [45] R. I. Joseph, Ballistic demagnetizing factor in uniformly magnetized cylinders, *Journal of applied physics* **37**, 4639 (1966).
- [46] V. Labinac, N. Erceg and D. Kotnik-Karuza, Magnetic field of a cylindrical coil, *Am. J. Phys.* **74**, 621 (2006).
- [47] Y. Z. Zhou, J. Guo, S. Cai, J. Y. Zhao, G. Guo, C. T. Lin, H. T. Yan, C. Huang, C. L. Yang, S. J. Long *et al.*, Quantum phase transition from superconducting to insulating-like state in a pressurized cuprate superconductor, *Nat. Phys.* **18**, 406 (2022).

- [48] B. Geisler, L. Fanfarillo, J. J. Hamlin, G. R. Stewart, R. G. Hennig and P. J. Hirschfeld, Optical properties and electronic correlations in La₃Ni₂O₇ bilayer nickelates under high pressure, arXiv:2401.04258 (2024).
- [49] Y. B. Liu, J. W. Mei, F. Ye, W. Q. Chen and F. Yang, s_{\pm} -Wave pairing and the destructive role of apical-oxygen deficiencies in La₃Ni₂O₇ under pressure, Physical Review Letters **131**, 6, 236002 (2023).
- [50] X. W. Yi, Y. Meng, J. W. Li, Z. W. Liao, J. Y. You, B. Gu and G. Su, Antiferromagnetic ground State, charge density waves and oxygen vacancies induced metal-insulator transition in pressurized La₃Ni₂O₇, arxiv:2403.11455 (2024).
- [51] J. Yang, H. Sun, X. Hu, Y. Xie, T. Miao, H. Luo, H. Chen, B. Liang, W. Zhu, G. Qu *et al.*, Orbital-dependent electron correlation in double-Layer nickelate La₃Ni₂O₇, arXiv:2309.01148 (2023).
- [52] Q. G. Yang, D. Wang and Q. H. Wang, Possible s_{\pm} -wave superconductivity in La₃Ni₂O₇, Physical Review B **108**, 5, L140505 (2023).
- [53] T. Kaneko, H. Sakakibara, M. Ochi and K. Kuroki, Pair correlations in the two-orbital Hubbard ladder: Implications for superconductivity in the bilayer nickelate La₃Ni₂O₇, Physical Review B **109** (2024).
- [54] Z. Luo, B. Lv, M. Wang and D.-X. Yao, High-T_c superconductivity in La₃Ni₂O₇ based on the bilayer two-orbital t-J model, arXiv:2308.16564 (2023).
- [55] W. Wu and Y.-Y. Zheng, Superconductivity in the bilayer two-orbital Hubbard mode, arXiv:2312.03605 (2023).
- [56] T. Xie, M. Huo, X. Ni, F. Shen, X. Huang, H. Sun, H. C. Walker, D. Adroja, D. Yu and B. Shen, Neutron scattering studies on the high-T_c superconductor La₃Ni₂O₇- δ at ambient pressure, arXiv:2401.12635 (2024).
- [57] N. S. Headings, S. M. Hayden, R. Coldea and T. G. Perring, Anomalous high-energy spin excitations in the high-T_c superconductor-parent antiferromagnet La₂CuO₄, Physical Review Letters **105**, 4, 247001 (2010).
- [58] P. C. Dai, Antiferromagnetic order and spin dynamics in iron-based superconductors, Rev. Mod. Phys. **87**, 855 (2015).
- [59] J. J. Zhang, H. Zheng, Y. S. Chen, Y. Ren, M. Yonemura, A. Huq and J. F. Mitchell, High oxygen pressure floating zone growth and crystal structure of the metallic nickelates R₄Ni₃O₁₀ (R = La, Pr), Physical Review Materials **4**, 14, 083402 (2020).
- [60] F. Li, N. Guo, Q. Zheng, Y. Shen, S. Wang, Q. Cui, C. Liu, S. Wang, X. Tao and G.-M. Zhang, Design and synthesis of three-dimensional hybrid Ruddlesden-Popper nickelate single crystals, arXiv:2312.08116 (2023).
- [61] H. Oh and Y. H. Zhang, Type-II t -J model and shared superexchange coupling from Hund's rule in superconducting La₃Ni₂O₇, Physical Review B **108**, 8, 174511 (2023).
- [62] H. Yang, H. Oh and Y.-H. Zhang, Strong pairing from small Fermi surface beyond weak coupling, arXiv:2309.15095 (2023).
- [63] S. Ryee, N. Witt and O. T. Wehling, Quenched pair breaking by interlayer correlations as a key to superconductivity in La₃Ni₂O₇, arXiv:2310.17465 (2024).

Supplementary Information: Pressure-driven right-triangle shape superconductivity in bilayer nickelate $\text{La}_3\text{Ni}_2\text{O}_7$

Jingyuan Li¹, Peiyue Ma¹, Hengyuan Zhang¹, Xing Huang¹, Chaoxin Huang¹, Mengwu Huo¹, Deyuan Hu¹, Zixian Dong¹, Chengliang He¹, Jiahui Liao¹, Xiang Chen¹, Tao Xie¹, Hualei Sun^{2,*}, Meng Wang^{1,*}

¹Center for Neutron Science and Technology, Guangdong Provincial Key Laboratory of Magnetoelectric Physics and Devices, School of Physics, Sun Yat-Sen University, Guangzhou, Guangdong 510275, China

²School of Science, Sun Yat-Sen University, Shenzhen, Guangdong 518107, China

*Email: sunhlei@mail.sysu.edu.cn; wangmeng5@mail.sysu.edu.cn

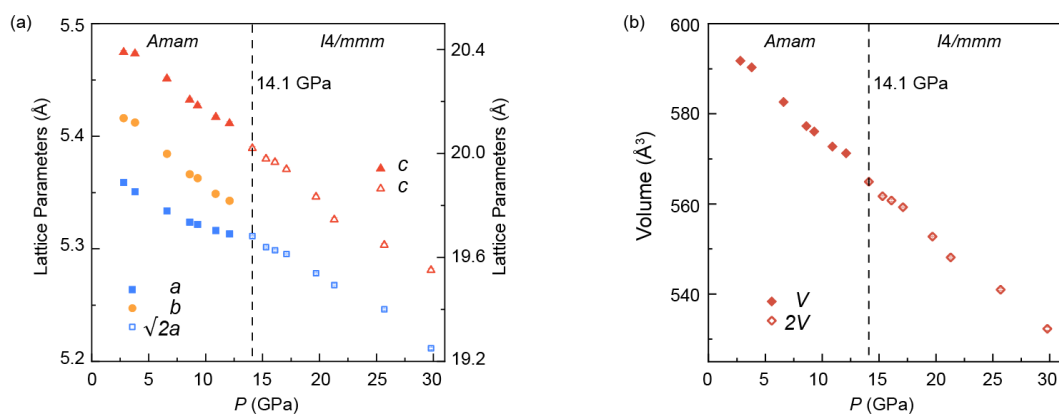


FIG. S1. (a) Lattice parameters and (b) Cell volume of $\text{La}_3\text{Ni}_2\text{O}_7$ as a function of pressure up to 29.8 GPa.

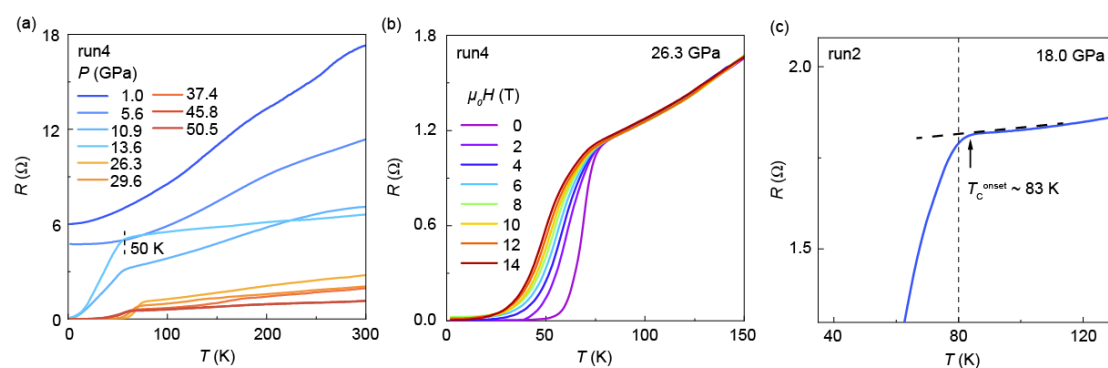


FIG. S2. (a) High-pressure resistance curves of run 4 measurements. Superconductivity emerges at 50 K under 10.9 GPa. (b) Field-dependent resistance at 26.3 GPa of run 4. The superconducting transition is gradually weakened by external fields. (c) Enlarged detail of the onset temperature at 18.0 GPa of run 2. The resistance starts to deviate from the linear curve approximately at 83 K.

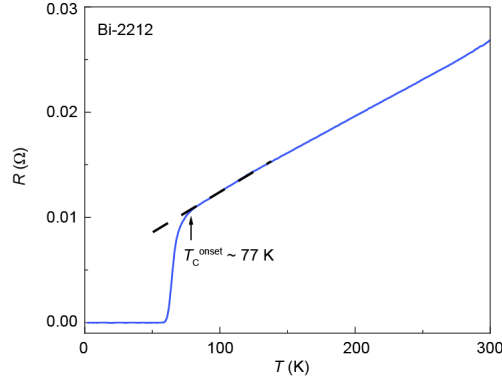


FIG. S3. Temperature dependence of the in-plane resistance of $\text{Bi}_2\text{Sr}_2\text{CaCu}_2\text{O}_{8+\delta}$ (Bi-2212) polycrystalline sample. The onset temperature is 77 K, consistent with the T_c determined by the dc magnetic susceptibility measurement.

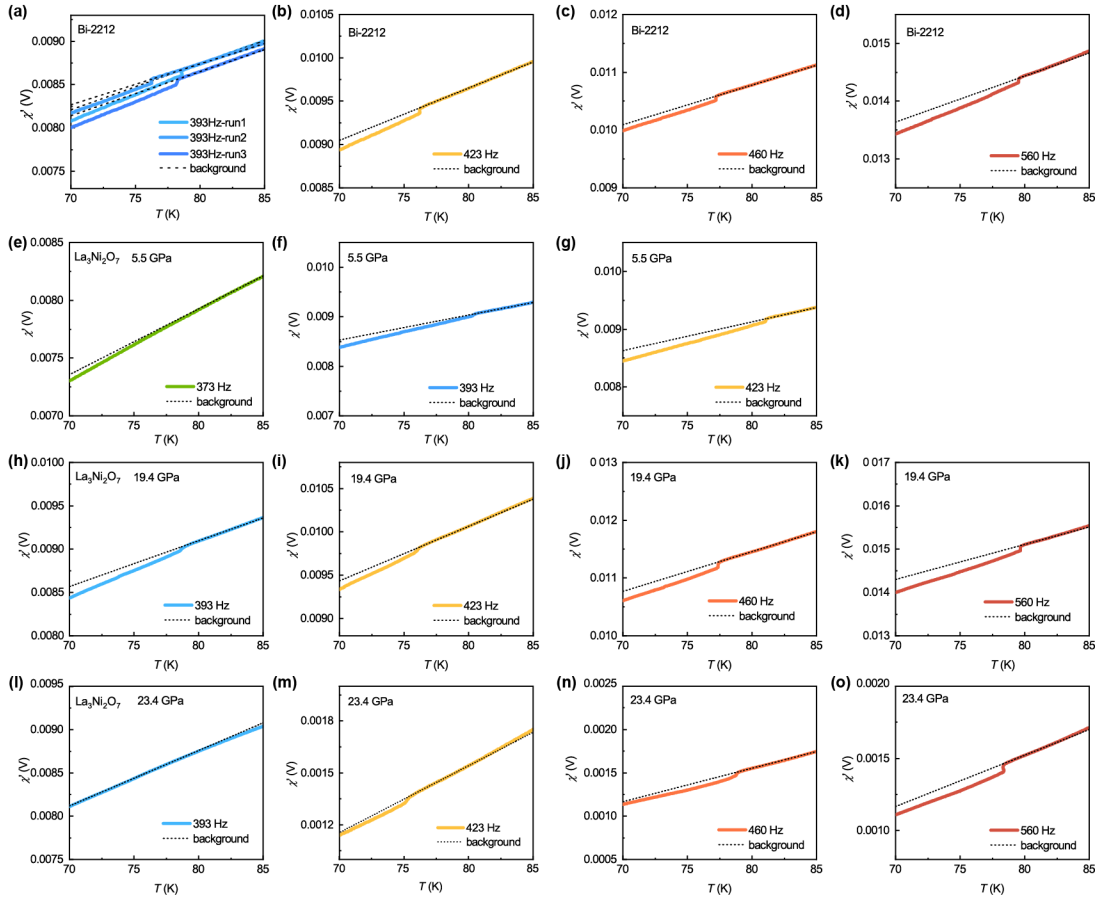


FIG. S4. Raw data of the real part of the ac magnetic susceptibility measurements. (a)-(d) Frequency dependence of the real part of the ac magnetic susceptibility of Bi-2212 at ambient pressure. (e)-(g) Similar measurements of $\text{La}_3\text{Ni}_2\text{O}_7$ at 5.5 GPa, (h)-(k) 19.4 GPa, and (l)-(o) 23.4 GPa.